

1 **Role of surface physicochemical properties of pipe materials**  
2 **on bio-clogging in leachate collection systems from a**  
3 **thermodynamic perspective**

4  
5 *Qian Wang<sup>†</sup>, Qianming Miao<sup>†</sup>, Xinwei Wang<sup>±</sup>, Tong Wang<sup>†</sup>, Qiyong Xu<sup>†,\*</sup>*

6 <sup>†</sup> School of Environment and Energy, Peking University Shenzhen Graduate School,  
7 University Town, Xili, Nanshan District, Shenzhen, 518055, PR China

8 <sup>±</sup> School of Advanced Materials, Peking University Shenzhen Graduate School,  
9 University Town, Xili, Nanshan District, Shenzhen, 518055, China

10

11

*Submitted to*

12

*Science of the Total Environment*

13

14

15

*\* Corresponding author.*

16

*Phone: 86-755-26033226, Fax: 86-755-26035332; Email: [qiyongxu@pkusz.edu.cn](mailto:qiyongxu@pkusz.edu.cn)*

1 **Role of surface physicochemical properties of pipe materials**  
2 **on bio-clogging in leachate collection systems from a**  
3 **thermodynamic perspective**

4  
5 *Qian Wang<sup>†</sup>, Qianming Miao<sup>†</sup>, Xinwei Wang<sup>±</sup>, Tong Wang<sup>†</sup>, Qiyong Xu<sup>†,\*</sup>*

6 <sup>†</sup> School of Environment and Energy, Peking University Shenzhen Graduate School,  
7 University Town, Xili, Nanshan District, Shenzhen, 518055, PR China

8 <sup>±</sup> School of Advanced Materials, Peking University Shenzhen Graduate School,  
9 University Town, Xili, Nanshan District, Shenzhen, 518055, China

10

11

*Submitted to*

12

*Science of the Total Environment*

13

14

15

*\* Corresponding author.*

16

*Phone: 86-755-26033226, Fax: 86-755-26035332; Email: [qiyongxu@pkusz.edu.cn](mailto:qiyongxu@pkusz.edu.cn)*

17

18 **Abstract**

19 Bio-clogging in pipes poses a significant threat to the operation of leachate  
20 collection systems. Bio-clogging formation is influenced by the pipe materials.  
21 However, the relationship between bio-clogging and the physicochemical properties of  
22 different pipe materials has not been clarified yet, especially from a thermodynamic  
23 aspect. In this study, the dynamic bio-clogging processes in pipes of different materials  
24 (high-density polyethylene (HDPE), polyvinyl chloride (PVC), polypropylene (PP),  
25 and polyethylene (PE)) were compared, and their correlation with the physicochemical  
26 properties was investigated. Results showed that the bio-clogging in HDPE and PVC  
27 pipes was more severe than that in PP and PE pipes. In bio-clogging development, the  
28 predominant factor changed from the surface roughness to the electron donor  
29 parameter ( $\gamma$ ). In the initial phase, the most severe bio-clogging was observed in the  
30 HDPE pipe, which exhibited the highest roughness ( $432\pm 76$  nm). In the later phase, the  
31 highest  $\gamma$  ( $2.2$  mJ/m<sup>2</sup>) and protein content ( $2623.1\pm 33.2$   $\mu$ g/cm<sup>2</sup>) were observed in the  
32 PVC simultaneously. Moreover, the interaction energy indicated that the bacteria could  
33 irreversibly and reversibly adhere to the HDPE, whereas irreversible adhesion was  
34 observed in the PVC, PP, and PE cases. The findings clarify the thermodynamic  
35 mechanism underlying bio-clogging behaviors and provide novel insights into the bio-  
36 clogging behaviors in pipes of different materials, which can facilitate the development  
37 of effective bio-clogging control strategies.

38 **Keywords:** Bio-clogging, Pipe materials, Leachate, Thermodynamic analysis,  
39 Interaction energy

## 40 1. **Introduction**

41 The clogging of leachate collection systems (LCSs) represents a collective  
42 environmental challenge in landfills. As a key component of LCSs, pipes are commonly  
43 used to collect and transport leachate to treatment facilities (Shaha et al., 2019).  
44 Different materials, such as high-density polyethylene (HDPE), polyvinyl chloride  
45 (PVC), polypropylene (PP), and polyethylene (PE), have been used to prepare pipes  
46 (Tarek and Daria, 2015). Many fields and laboratory studies have indicated varying  
47 degrees of bio-clogging in pipes made of different materials (Liu and Liu, 2021; Rowe  
48 and Yu, 2012; Tang et al., 2018). For instance, Li et al. (2021) reported that the bacterial  
49 amount related to bio-clogging in PVC was higher than that in HDPE. In general, bio-  
50 clogging decreases the hydraulic conductivity of pipes and leachate flow rate, which  
51 increases the possibility of LCSs clogging. LCSs clogging poses a threat to landfill  
52 stability and may lead to the pollution of the surrounding environment (Feng et al., 2020;  
53 Wu et al., 2018). Therefore, exploring the bio-clogging mechanisms related to different  
54 pipe materials in LCSs is critically important to controlling clogging in landfills.

55 Although many researchers have focused on the relationship between bio-clogging  
56 and physicochemical properties (e.g. surface free energy, Zeta potential, interaction  
57 energy) of different pipe materials in domestic wastewater treatment plants, the bio-  
58 clogging mechanisms in landfills have not been extensively investigated. Zhang et al.  
59 (2019) noted that in wastewater treatment plants, the surface free energy and Zeta  
60 potential could influence bacteria adhesion behaviors in different pipe materials.  
61 Additionally, the interaction energy of pipe materials could influence the secretion of

62 protein and polysaccharides, which represent the main components of extracellular  
63 polymeric substances (EPSs) (Teng et al., 2022). Both bacteria adhesion and EPSs  
64 secretion are key processes in bio-clogging development (Carrel et al., 2018; Wang et  
65 al., 2021b). Notably, the bio-clogging characteristics are influenced by not only the pipe  
66 materials but also the type of wastewaters (e.g. sewage, leachate). Leachate is a type of  
67 heterogeneous wastewater with various compositions and contains high-level pollutants,  
68 i.e., bacteria, organic matter, and inorganic ions, which render the bio-clogging  
69 phenomena complex (Luo et al., 2020; Anand et al., 2022). Our previous study  
70 illustrated that the leachate characteristics could change the bio-clogging components  
71 and microbial communities (Wang et al., 2021b). Hence, the relationship between bio-  
72 clogging and the physicochemical properties of pipe materials exposed to leachate must  
73 be explored to facilitate the control of bio-clogging behaviors pertaining to leachate.

74       Recently, different thermodynamic theories have been used to describe and predict  
75 the adhesion behaviors between bio-clogging constituents and material surfaces (Zeng  
76 et al., 2022; Wu et al., 2020). The extended Derjaguin–Landau–Verwey–Overbeek  
77 (XDLVO) theory has been regarded as the ideal theory for describing the bio-clogging-  
78 related adhesion behaviors related to materials encountered in domestic wastewater  
79 treatment (Habimana et al., 2014; Yin et al., 2020). The XDLVO theory is based on  
80 acid-based, van der Waals, and electrostatic double-layer interaction energies  
81 (Somathilake and Hettiaratchi, 2012). Based on the XDLVO theory, Yongabi et al.  
82 (2020) reported that the adhesive behavior between bacteria and the material surface is  
83 controlled by the electrostatic double-layer interaction energy at the initial contact,

84 whereas stable adhesion is driven by the van der Waals energy. In addition, the XDLVO  
85 theory has been to interpret the dynamic adhesion behavior of protein and  
86 polysaccharides on the membrane surface in domestic wastewater treatment (Teng et  
87 al., 2022). However, to the best of the authors' knowledge, little research has been  
88 conducted to identify the relationship between the bio-clogging and physicochemical  
89 properties of pipe materials subjected to leachate, especially considering the influence  
90 of the leachate dynamic characteristics on the dynamic evolution of bio-clogging.

91 Therefore, this study was aimed at clarifying the influence of the physicochemical  
92 properties of different pipe materials subjected to leachate on the dynamic evolution of  
93 bio-clogging and the related thermodynamic mechanisms. Experimental  
94 characterizations based on confocal laser scanning microscopy (CLSM), colony-  
95 forming unit (CFU) measurements, and 16S rRNA gene sequencing were performed to  
96 characterize the dynamic changes in bio-clogging. The physicochemical properties  
97 (roughness, hardness, Zeta potential, and surface energy) of four common kinds of pipe  
98 materials were compared. Moreover, the XDLVO theory and redundancy analysis  
99 (RDA) was used to describe the effects of physicochemical properties on bio-clogging.  
100 The findings can provide novel thermodynamic insights into leachate-related bio-  
101 clogging, thereby promoting the development of bio-clogging control strategies.

## 102 **2. Material and methods**

### 103 **2.1 Pipe materials and chemicals**

104 Four most commonly used pipe materials, i.e., HDPE, PVC, PP, and PE, were  
105 considered in this study (Alimi et al., 2018). HDPE, PVC, PP, and PE were purchased

106 from markets in Shenzhen, China. With reference to a previous study (Cai et al., 2019),  
107 the pipe materials were cut into 1.0×1.0 cm squares using sterile scissors, washed with  
108 ethanol and ultrapure water two times, and air-dried for further analyses. As illustrated  
109 in Fig. S1, the FTIR spectra of these four pipe materials are compared. All the chemicals  
110 were purchased from Xilong Scientific (Shantou, China). Unless specified, all  
111 chemicals were dissolved in ultrapure water obtained from a Milli-Q ultrapure water  
112 purification system (Millipore, USA).

## 113 **2.2 Characterizations of pipe materials**

114 The physicochemical surface properties of the pipes, including the roughness,  
115 hardness, Zeta potential, and contact angle were analyzed. The pipe roughness was  
116 determined through atomic force microscopy (AFM) (Dimension Icon, Bruker, USA)  
117 with a scan range of 50.0×50.0 μm, and a scanning speed of 0.4-0.6 Hz. Specifically,  
118 AFM images were analyzed using the NanoScope Analysis software to calculate the  
119 roughness. Measurements for each pipe material were conducted in triplicate. The pipe  
120 hardness was determined using a Shore durometer (LXD-D, Shanghai Siwei Instrument  
121 Manufacturing Co., China) according to the ASTM D2240D standard (Cai et al., 2019).  
122 For each type of pipe material, measurements were obtained for at least six sites. The  
123 Zeta potentials of the pipe materials and leachate were measured using a Zetasizer  
124 (Nano ZS, Malvern, UK), based on the electrophoretic light scattering  
125 spectrophotometer method. The pipe materials were crushed and grinded as  
126 pretreatment for the Zeta potential analysis. Each measurement was performed at least  
127 six times at ambient temperature (25±2°C). The major functional groups of pipe

128 materials were determined through Fourier transform infrared spectroscopy (FTIR)  
 129 (IRTracer-100, Shimadzu, Japan) between 400 cm<sup>-1</sup> and 3600 cm<sup>-1</sup> (Fig. S1).

130 The contact angle of the probe liquid was measured using a contact angle meter,  
 131 based on the drip-stop method (ThetaLite, Biolin Attention, Sweden). Ultrapure water,  
 132 diiodomethane, and ethylene glycol were selected as the probe liquids to derive the  
 133 surface tension components of the solids. The contact angle for one pipe material was  
 134 measured based on five samples. The contact angle for the bacteria was measured  
 135 through bacterial lawns, obtained by filtering the leachate through a Millipore filter  
 136 (0.22 μm) (Zhang et al., 2019). The total surface tension  $\gamma$  contained two components:  
 137 an apolar Lifshitz-van der Waals component,  $\gamma^{LW}$ ; and a polar acid-based component,  
 138  $\gamma^{AB}$ . The acid-based component consisted of an electron acceptor ( $\gamma^+$ ) and electron  
 139 donator ( $\gamma^-$ ). Therefore, the total surface tension of the pipe material and bacteria was  
 140 calculated as follows (Liu et al., 2007; Van Oss, 1994):

$$141 \quad \gamma = \gamma^{LW} + \gamma^{AB} = \gamma^{LW} + 2\sqrt{\gamma^+ \gamma^-}$$

142 (1)

$$143 \quad (1 + \cos \theta)\gamma_L = 2\left(\sqrt{\gamma_L^{LW} \gamma_S^{LW}} + 2\sqrt{\gamma_S^+ \gamma_L^-} + \sqrt{\gamma_L^+ \gamma_S^-}\right)$$

144 (2)

145 Where  $\theta$  is the contact angle of three polar liquids (ultrapure water,  
 146 diiodomethane, and ethylene glycol).  $\gamma_L$  is the Lifshitz-van der Waals, electron  
 147 acceptor, and electron donator parameters of different probe liquids (Table S1).  $\gamma_S^{LW}$   
 148 and  $\gamma_L^{LW}$  represent the Lifshitz-van der Waals parameter of the pipe material surface  
 149 and probe liquid, respectively.  $\gamma_S^+$  and  $\gamma_L^+$  represent the electron acceptor parameter



150 of the pipe surface and probe liquid, respectively.  $\gamma_{\bar{S}}$  and  $\gamma_{\bar{L}}$  represent the electron  
151 donator parameter of the pipe surface and probe liquid, respectively.

### 152 **2.3 Preparation of bacterial strains**

153 The bacterial strains and leachate were collected from the simulated municipal  
154 solid waste (MSW) landfill reactor. The synthetic MSW was composed of 65% food  
155 waste, 10% paper, 10% sand, 10% pipe material, and 5% others (glass and metals). The  
156 pH, conductivity, and ammonia concentration of leachate were 5.28, 6.65 mS/cm, and  
157 460 mg/L, respectively (Table S2). The community structures of leachate were detected  
158 by the 16 S rRNA with the primer sets of 338F (5'-ACTCCTACGGGAGGCAGCAG-  
159 3') and 806R (5'-GGACTACHVGGGTWTCT-3'). Polymerase chain reactions (PCR)  
160 reactions were performed in a mixture containing a buffer, primer, and template DNA.  
161 The PCR products were extracted from a 2% agarose gel and further purified and  
162 quantified. The purified amplicons were paired-end sequenced on an Illumina MiSeq  
163 platform according to the standard protocols specified by Majorbio Bio-Pharm  
164 Technology Co. Ltd.

### 165 **2.4 Bio-clogging formation experiment**

166 A bio-clogging formation experiment was performed in 200 mL beakers. The  
167 experimental groups contained 50 mL leachate and 6 pieces of sterilized pipe materials,  
168 whereas the control groups contained 50 mL sterilized ultrapure water and 6 pieces of  
169 sterilized pipe materials. Each beaker was flushed with nitrogen for 10 min and rapidly  
170 sealed with a frosted cover to maintain anaerobic conditions. Finally, all the beakers  
171 were incubated in a thermostat at  $35\pm 2^{\circ}\text{C}$ . According to previous studies (Wang et al.,

172 2021a; Wang et al., 2022), the pipe materials in the four beakers were extracted on days  
173 1 and 14, representing phases I and II, respectively, for further analyses. Phase I  
174 corresponded to the initial phase of bio-clogging formation, mainly caused by bacteria  
175 adsorption (Tang et al., 2018). Phase II represented the later phase of bio-clogging  
176 formation, with increased EPS contents (Wang et al., 2022).

## 177 **2.5 Analysis of bio-clogging characteristics**

178 The bio-clogging materials were characterized in terms of morphology,  
179 component distribution, EPS contents, and bacterial contents. The morphology was  
180 analyzed by scanning electron microscopy (SEM) (Supra®55, Lecia, Germany) at 15  
181 kV. The SEM samples were prepared according to a previous study (Wang et al.,  
182 2021b). Firstly, the pipe materials were fixed using a primary fixative (2.5%  
183 glutaraldehyde in 0.1 M phosphate buffer). Subsequently, the pipe materials were  
184 dehydrated with increasing concentrations of ethanol solutions (30%, 50%, 70%, 85%,  
185 90%, and 100%) and substituted with isoamyl acetate. The samples were frozen at -20°C  
186 and -80°C for 4 h, respectively. Finally, the freeze-dried samples were sputter-coated  
187 with Au and imaged using SEM.

188 The distribution of the bio-clogging components was detected by CLSM (AIR,  
189 Nikon, Japan). Four pipe coupons were obtained from the clogged pipe sample by  
190 cutting with sterile scissors. The coupons were stained with SYTO 9 and propidium  
191 iodide (PI) for the detection of live cells and dead cells, respectively. The concentrations  
192 of SYTO 9 and PI were 3.34 and 20  $\mu\text{M}$ , respectively. The stained coupons were  
193 incubated in the dark for 30 min and then rinsed with 0.1 M phosphate buffer solution

194 (PBS) three times before imaging. The images were further analyzed using NIS-  
195 Element and Image J (National Institute of Health, USA).

196 The EPS was extracted by a heating method as previously described (Zhang et al.,  
197 2009). The pipe materials were put into 2 mL PBS and ultrasonic for 10 min, followed  
198 by heat treatment at 80°C for 30 min. The heat-treated samples were subjected to 10  
199 min of ultrasonication and then centrifuged at 10000 rpm for 10 min (20°C). The  
200 polysaccharide and protein contents were detected using phenol-sulfuric acid and  
201 diquinoline formic acid methods, respectively (Dubois et al., 1956; Osnes et al., 1993).

202 The bacterial contents were measured using the CFU method. After the bio-  
203 clogging experiments, the pipe materials with attached bacteria were suspended and  
204 gently rinsed with PBS solution three times to remove the culture medium. For the  
205 remaining attached bacteria, the pipe materials were placed in 5 mL PBS, and the  
206 mixture was vigorously shaken manually and by using a vortex for 30 s. Finally, a 50  
207  $\mu$ L sample was dropped onto beef-extract peptone with a sterile pipette and incubated  
208 at  $35\pm 2^\circ\text{C}$  for 24 h. The colonies on the beef-extract peptone plates were counted to  
209 determine the number of viable bacteria in each sample. Replicated experiments were  
210 performed for the colonies on the plates for each sample (n=4). Quantitative PCR (Q-  
211 PCR) was conducted to analyze the bacterial density using primer sets of 338F (5'-  
212 ACTCCTACGGGAGGCAGCAG-3')/806R (5'-GGACTACHVGGGTWTCTAAT-  
213 3'). The reactions were implemented using an ABI7300 real-time PCR system (Applied  
214 Biosystems, USA). The community structures of bio-clogging were detected as  
215 described in Section 2.3.

216 **2.6 Thermodynamic evaluation of the interaction energy**

217 The Gibbs adhesion energy between the pipe materials and bacteria in leachate can  
 218 be calculated using the XDLVO approach (Teng et al., 2019). The total adhesive energy  
 219 primarily consists of Lifshitz-van der Waals energy,  $G_{adh}^{LW}$ , acid-based energy,  $G_{adh}^{AB}$ ,  
 220 and electrostatic double-layer interaction energy,  $\Delta G_{adh}^{EL}$ , which can be calculated by  
 221 (Wu et al., 2020; Xu et al., 2016):

222 
$$\Delta G_{adh} = \Delta G_{adh}^{LW} + \Delta G_{adh}^{AB} + \Delta G_{adh}^{EL}$$
  
 223 (3)

224 
$$\Delta G_{adh}^{LW} = -2(\sqrt{\gamma_b^{LW}} - \sqrt{\gamma_l^{LW}})(\sqrt{\gamma_s^{LW}} - \sqrt{\gamma_l^{LW}})$$
  
 225 (4)

226 
$$\Delta G_{adh}^{AB} = 2(\sqrt{\gamma_b^+} - \sqrt{\gamma_s^+})(\sqrt{\gamma_b^-} - \sqrt{\gamma_s^-}) - 2(\sqrt{\gamma_b^+} - \sqrt{\gamma_l^+})(\sqrt{\gamma_b^-} - \sqrt{\gamma_l^-})$$
  
 227 
$$- 2(\sqrt{\gamma_s^+} - \sqrt{\gamma_l^+})(\sqrt{\gamma_s^-} - \sqrt{\gamma_l^-})$$
  
 228 (5)

229 
$$\Delta G_{adh}^{EL} = \frac{\epsilon\kappa(\zeta_b^2 + \zeta_s^2)}{2} \left[ 1 - \coth \kappa d_0 + \frac{2\zeta_b\zeta_s}{\zeta_b^2 + \zeta_s^2} \operatorname{csch} \kappa d_0 \right]$$
 (6)

230 
$$\kappa = \sqrt{\frac{4N_A e^2 I}{\epsilon K T}}$$
 (7)

231 Where subscript  $b$ ,  $s$ , and  $l$  mean bacteria, pipe material, and leachate,  
 232 respectively.  $\zeta$  and  $\kappa$  mean Zeta potential (mV) and reciprocal Debye length ( $\text{nm}^{-1}$ ),  
 233 respectively.  $d_0$  represents the minimum separation distance (nm) within two flat  
 234 surfaces.  $N_A$  is the Avogadro constant,  $e$  is the elementary charge of an electron,  $I$  is  
 235 ionic strength,  $K$  is the Boltzmann constant,  $\epsilon$  is the dielectric constant, and  $T$  is  
 236 temperature. The value of different parameters used in this study was presented in Table  
 237 S3. In this study, 0.2 M and 0.158 nm were set as the ionic strength and minimum

238 separation distance (Chen et al., 2012; Townsend, 2015). The Gibbs adhesion energy  
239 was calculated by the average values of different parameters.

240 The interaction energy between the bacteria and pipe materials was calculated  
241 assuming the entities as two surfaces. Similar assumptions have been used in the  
242 previous study (Teng et al., 2019). The XDLVO theory represents the primary method  
243 to calculate the interaction energy for the two surfaces (Van Oss, 1994). Accordingly,  
244 the total interaction energy ( $\Delta G^{TOT}$ ) can be calculated as follows:

$$245 \quad \Delta G^{TOT}(d) = \Delta G^{LW}(d) + \Delta G^{EL}(d) + \Delta G^{AB}(d)$$

246 (8)

$$247 \quad \Delta G^{LW}(d) = S\Delta G_{adh}^{LW} \frac{d_0^2}{d^2} \quad (9)$$

$$248 \quad \Delta G^{AB}(d) = S\Delta G_{adh}^{AB} \exp\left(\frac{d_0 - d}{\lambda}\right) \quad (10)$$

$$249 \quad \Delta G^{EL}(d) = S\epsilon\kappa\zeta_b\zeta_s \left[ \frac{(\zeta_b^2 + \zeta_s^2)}{2\zeta_b\zeta_s} (1 - \coth \kappa d) + \frac{1}{\sinh \kappa d} \right] \quad (11)$$

250 Where  $S$  is the interaction surface area between bacteria and pipe materials ( $m^2$ ).

## 251 2.7 Statistical analysis

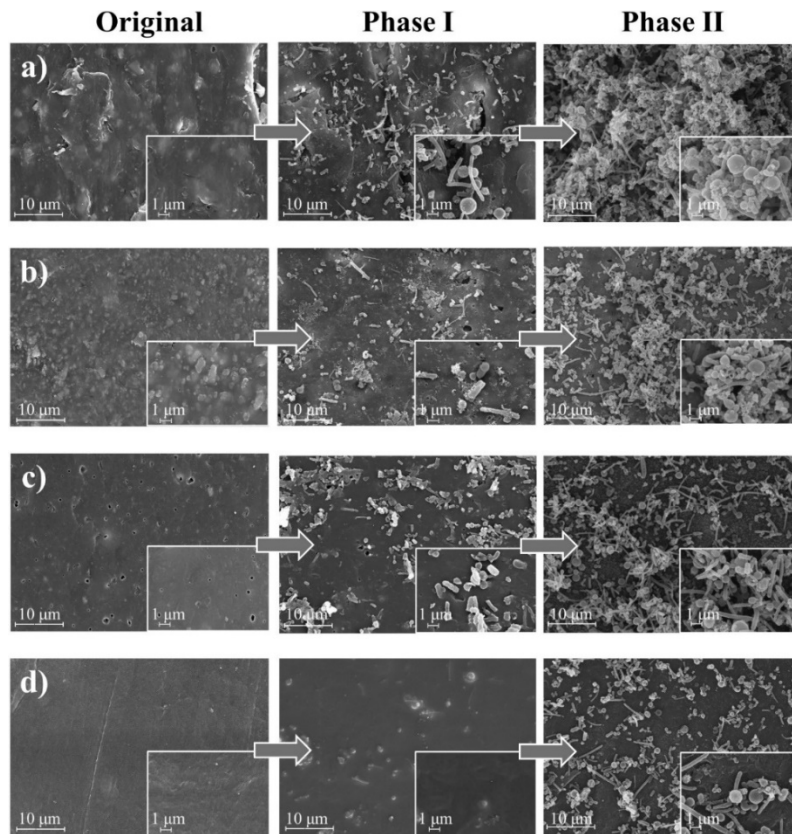
252 The results were expressed as mean  $\pm$  standard deviation values. One-way analysis  
253 of variance was performed to evaluate the statistical differences. All the significance  
254 analyses were performed using the PASW 18.0 software (SPSS Inc., USA), and a p-  
255 value of  $<0.05$  was considered to indicate statistical significance (Table S4-5).  
256 Redundancy analysis (RDA) was performed to clarify the relationship between the bio-  
257 clogging characteristics and pipe surface physicochemical properties using Canoco  
258 (Version 5.02, ScientiaPro, Hungary). A person's correlation between two parameters  
259 among different surface physicochemical properties and bio-clogging characteristics

260 was calculated and compared.

### 261 **3. Results and discussion**

#### 262 **3.1 Characteristics and composition of bio-clogging**

263 Fig. 1 shows the morphological characterization of different pipe materials. In  
264 terms of the bare pipe materials, the surfaces of HDPE and PVC were rough and coarse,  
265 whereas those of PP and PE were smooth. In phase I, the bacteria adsorbed on the  
266 surface of HDPE, PVC, and PP exhibited a rod-like and spherical structure with several  
267 attached bacteria and broken cells. Significant bacterial adhesion was not observed on  
268 the PE surface. The number of clogged materials in the four pipe materials considerably  
269 increased from phase I to phase II. The maximum amount of bacteria was observed on  
270 the HDPE surface, followed by the PVC and PP, and the PE exhibited the least amount  
271 of bacteria. These results indicated the clogging extent was associated with the pipe  
272 materials and phases, consistent with a previous study that highlighted that the clogging  
273 extent was positively correlated with the phase development (Ko et al., 2019). The  
274 bacteria could adhere to both rough and smooth pipe material surfaces by secreting  
275 EPSs to attach with the surface (Ganesan et al., 2022). Overall, the bacteria could  
276 develop bio-clogging on different pipe material surfaces with colonization ability, such  
277 as bacterial growth and EPSs secretion.

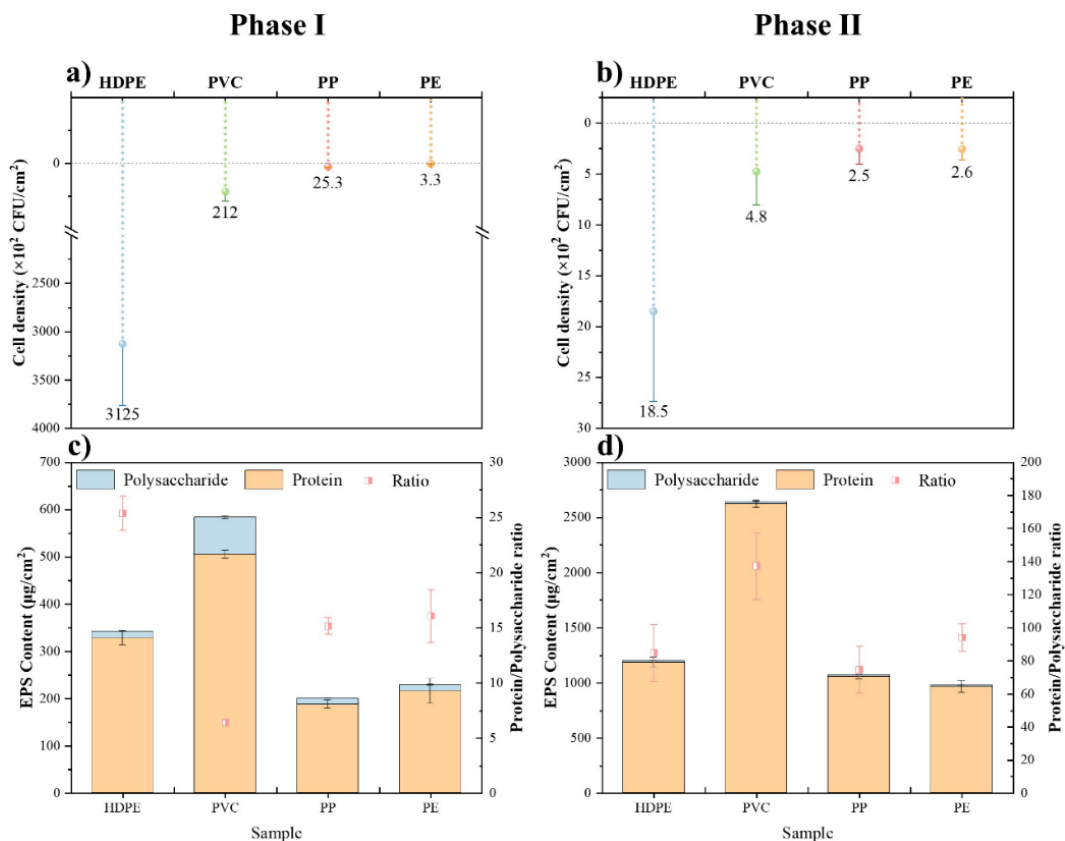


278

279 **Fig. 1** Surface morphology of different pipe materials in different phases. a) HDPE, b) PVC, c) PP,  
 280 d) PE.

281 As illustrated in Fig. 2, the bacteria density and EPS contents differed across the  
 282 pipe materials and phases. In phase I, the maximum cell density corresponded to HDPE  
 283 ( $3.1 \times 10^5 \pm 0.6 \times 10^5$  CFU/cm<sup>2</sup>), followed by PVC ( $2.1 \times 10^4 \pm 0.7 \times 10^4$  CFU/cm<sup>2</sup>), PP ( $2.5$   
 284  $\times 10^3 \pm 0.3 \times 10^3$  CFU/cm<sup>2</sup>), and PE ( $3.3 \times 10^2 \pm 1.2 \times 10^2$  CFU/cm<sup>2</sup>). Similar trends were  
 285 observed in phase II, although the cell density for the different pipe materials in phase  
 286 II was 1–2 orders of magnitude lower than those in phase I. In contrast, the total EPSs  
 287 content increased from phase I to phase II. In phase I, the EPS content ranged from  
 288  $199.7 \pm 9.1$  to  $583.4 \pm 11.1$  μg/cm<sup>2</sup>. Notably, EPSs were the main component of bio-  
 289 clogging in phase II, with contents ranging from  $973.8 \pm 51.6$  to  $2642.6 \pm 36.2$  μg/cm<sup>2</sup>.  
 290 These results suggested that the protein and polysaccharides contents increased with

291 the increasing phase, and the protein content was higher than that of the polysaccharides.  
 292 The proteins, secreted by bacteria, aggregated in response to the bacterial adhesion to  
 293 form EPSs and mediate the bacterial contacts, leading to an increase in the thickness of  
 294 bio-clogging (Flemming and Wingender, 2010). In addition, the EPSs secretion and  
 295 bacterial adhesion were associated with the physicochemical properties of the pipe  
 296 surface, such as the roughness, charge, and interaction energy (Teng et al., 2019). For  
 297 example, the highest EPSs contents were observed in PVC, whereas the HDPE  
 298 corresponded to the highest cell density. The cell density of PE did not change  
 299 considerably, although the cell densities of HDPE, PVC, and PP decreased from phase  
 300 I to phase II. These results also indicated that the physicochemical properties of pipe  
 301 materials could change microbial activities.



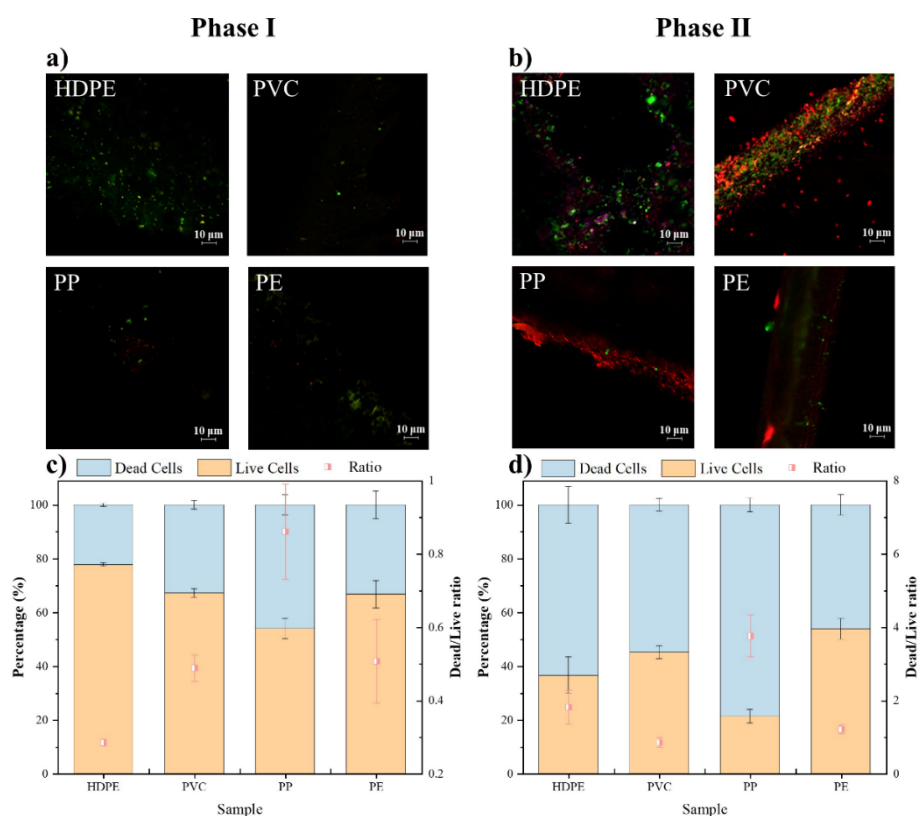
302  
 303 **Fig. 2** Attached cell density for different pipe materials. a) phase I, b) phase II. EPS contents and



304 protein/ polysaccharide ratios of different pipe materials. c) phase I, d) phase II.

305 Fig. 3 shows the fluorescent staining results of live and dead bacteria identified  
306 from different pipe materials. The live and dead bacteria were unevenly distributed on  
307 the surface of pipe materials (Fig. 3a, b). In phase I, the live bacteria (green) were the  
308 main contributors to bio-clogging, accounting for  $54.0\pm 3.8$  to  $77.8\pm 0.6\%$  of the total  
309 content (Fig. 3c). The percentage of live cells in the HDPE ( $77.8\pm 0.6\%$ ) was the highest,  
310 consistent with the highest cell density observed for the HDPE (Fig. 2a). In contrast, a  
311 highly dense red assembly was observed in phase II, suggesting the dominant presence  
312 of dead bacteria (Fig. 3d). The main component of bio-clogging changed from live  
313 bacteria to dead bacteria and EPSs in the bio-clogging development process (Meng et  
314 al., 2017). The percentage of live bacteria (Phase I) exhibited the following decreasing  
315 order: HDPE>PVC>PE>PP. The percentage of dead bacteria the phase I exhibited the  
316 following decreasing order: PP>HDPE>PVC>PE. These results highlighted that the  
317 physicochemical properties of pipe materials changed the distribution of bio-clogging  
318 under the same phase. Fig. S2 shows the bacterial communities in different pipe  
319 materials. In phase I, the main bacteria in the HDPE, PVC, and PP cases were  
320 *Proteobacteria* (57.1%), *Firmicutes* (46.4%), and *Actinobacteria* (40.4%), respectively.  
321 The bacteria in the case of PE mainly consisted of *Firmicutes* (34.2%) and  
322 *Actinobacteria* (32.9%). In other words, *Proteobacteria*, *Firmicutes*, and  
323 *Actinobacteria* exhibited strong adaptability and broad ubiquity in the bio-clogging and  
324 were abundantly present in the leachate (Xu et al., 2017). The physicochemical  
325 properties of the different pipe materials changed the bacterial communities in the bio-

326 clogging (Yan et al., 2022). The predominant bacteria for different pipe materials  
 327 changed from phase I to phase II. For example, the main bacteria for HDPE in phase II  
 328 were *Actinobacteria* (35.0%). In addition, a significant change was not observed in the  
 329 leachate characteristics among different pipe materials (Table S6), suggesting the pipe  
 330 material could not change the leachate characteristics and bio-clogging phases. Overall,  
 331 these results indicated that the introduction of differences in the species across bio-  
 332 clogging was a dynamic process related to the pipe materials and bio-clogging phases.

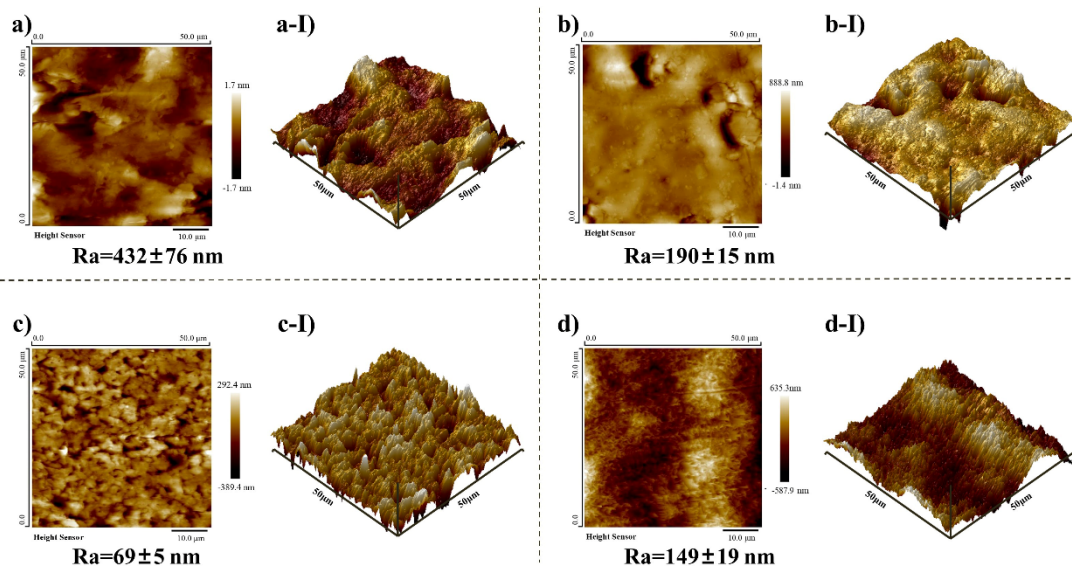


333  
 334 **Fig. 3** Representative CLSM images of bio-clogging in different pipe materials. a) phase I, b)  
 335 phase II. Live cells (green), dead cells (red). Distribution of live cells and dead cells in different  
 336 pipe materials. c) phase I, d) phase II.

### 337 3.2 Effects of physicochemical properties on the bio-clogging

338 The morphology and roughness of the pipe materials were visualized through

339 AFM (Fig. 4). As illustrated in Fig. 4, HDPE exhibited the highest average roughness  
 340 ( $432\pm 76$  nm), followed by the PVC ( $190\pm 15$  nm), PE ( $149\pm 19$  nm), and PP ( $69\pm 5$  nm).  
 341 The roughness influenced the contact area between the bacteria and the surface, thereby  
 342 affecting the bacterial adhesion (Yang et al., 2022). Notably, although the roughness of  
 343 PE was higher than that of PP, the less bio-clogging formation was observed in PE  
 344 compared to that in PP (Fig. 1 and 2). Thus, the surface roughness likely did not  
 345 represent the main factor for the bio-clogging formation in different pipe materials. This  
 346 observation is also supported by a previous study that highlighted that nanoscale surface  
 347 roughness could not provide micro crevices that could function as niches for bacteria  
 348 (Sousa et al., 2009). However, several recent studies have indicated that a high  
 349 roughness can influence the interaction force between bio-clogging (bacteria) and the  
 350 interface surface and decrease the interaction energy barrier between the two interacting  
 351 bodies (Bradford et al., 2018), thereby generating more favorable conditions for the  
 352 interaction. Thus, in this study, the effect of roughness on bio-clogging formation was  
 353 further evaluated, as described in Section 3.3.



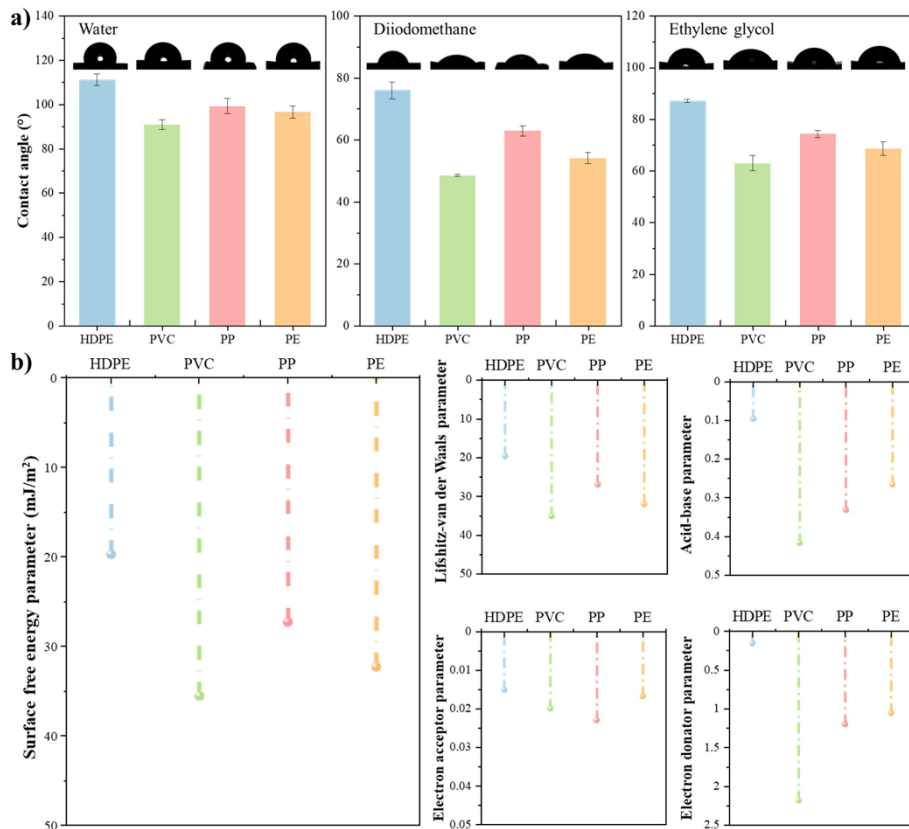
354

355 **Fig. 4** AFM deflection images and adhesion force measurements for different pipe materials. a)  
356 HDPE, b) PVC, c) PP, d) PE.

357 The surface hardness of the pipe materials could influence bacterial adhesion  
358 because hard semi-solid surfaces are expected to limit bacterial swarming (Kamatkar  
359 and Shrout, 2011; Cai et al., 2019). As illustrated in Fig. S3a), the surface hardness of  
360 HDPE ( $64.0\pm 0.5$  HD) and PVC ( $82.8\pm 0.5$  HD) was lower than those of PE ( $96.2\pm 0.4$   
361 HD) and PP ( $98.4\pm 0.2$  HD). PE and PP exhibited lower bacterial adhesion than HDPE  
362 and PVC. This finding indicated that the amount of bio-clogging formation was  
363 positively correlated with the surface hardness, consistent with previously reported  
364 findings (Cai et al., 2019). Moreover, the surface charge could affect bio-clogging  
365 formation through electrostatic interactions (Yang et al., 2022). The HDPE exhibited a  
366 significant negative charge, with a Zeta potential of  $-21.2\pm 0.3$  mV (Fig. S3b). The  
367 differences in the Zeta potential of PP and PE were not statistically significant ( $P>0.05$ ).  
368 The bacteria used in this study had a Zeta potential of  $-7.8\pm 0.8$  mV. These results  
369 indicated that the electrostatic interaction does not considerably influence the bio-  
370 clogging formation. To clarify the bio-clogging formation behavior between the  
371 bacteria and pipe materials, the thermodynamic approach and XDLVO theory were  
372 used to evaluate the contact angle, surface free energy, and Gibbs adhesion energy.

373 The contact angles were measured to investigate the hydrophilicity/  
374 hydrophobicity of the pipe materials (Fig. 5). As illustrated in Fig. 5a, the water contact  
375 angle of all pipe materials was more than  $90^\circ$ , suggesting that all pipe materials were  
376 hydrophobic. Notably, the maximum water contact angle corresponded to HDPE

377 (111.2±2.7° , P<0.01). Similar trends were also observed in other probe liquids,  
378 including diiodomethane and ethylene glycol. These contact angles were used to  
379 calculate the surface free energy of the pipe materials. As illustrated in Figure 5b, the  
380 minimum total surface energy ( $\gamma$ ) corresponded to HDPE (19.66 mJ/m<sup>2</sup>), followed by  
381 PP (27.23 mJ/m<sup>2</sup>), PE (31.95 mJ/m<sup>2</sup>), and PVC (35.49 mJ/m<sup>2</sup>). The Lifshitz–van der  
382 Waals parameter was noted to be the main contributor to the total surface energy for  
383 different pipe materials. These results indicated that HDPE corresponded to the lowest  
384 surface energy and most severe bio-clogging formation. Notably, our results were in  
385 contrast with those of previous studies that indicated that the bacteria adhesion was  
386 positively correlated with the surface energy (Merghni et al., 2016; Mohiuddin et al.,  
387 2011). As mentioned previously, HDPE corresponded to the highest roughness (Fig. 4).  
388 In general, for hydrophobic pipe materials, a larger contact angle corresponds to a  
389 rougher surface and more functional groups (Niu et al., 2021). In this context, the HDPE  
390 contained more carbonyl groups, as confirmed by the result of FTIR at wavelengths of  
391 1600–1900 cm<sup>-1</sup> (Fig. S1) (Syranidou et al., 2017). Overall, bio-clogging formation is  
392 a complex process influenced by different physicochemical properties, such as  
393 roughness, hardness, surface charge, and hydrophilicity. However, the effect and  
394 mechanisms of hydrophobicity and surface free energy of pipe materials on the bio-  
395 clogging need to be extensively investigated.



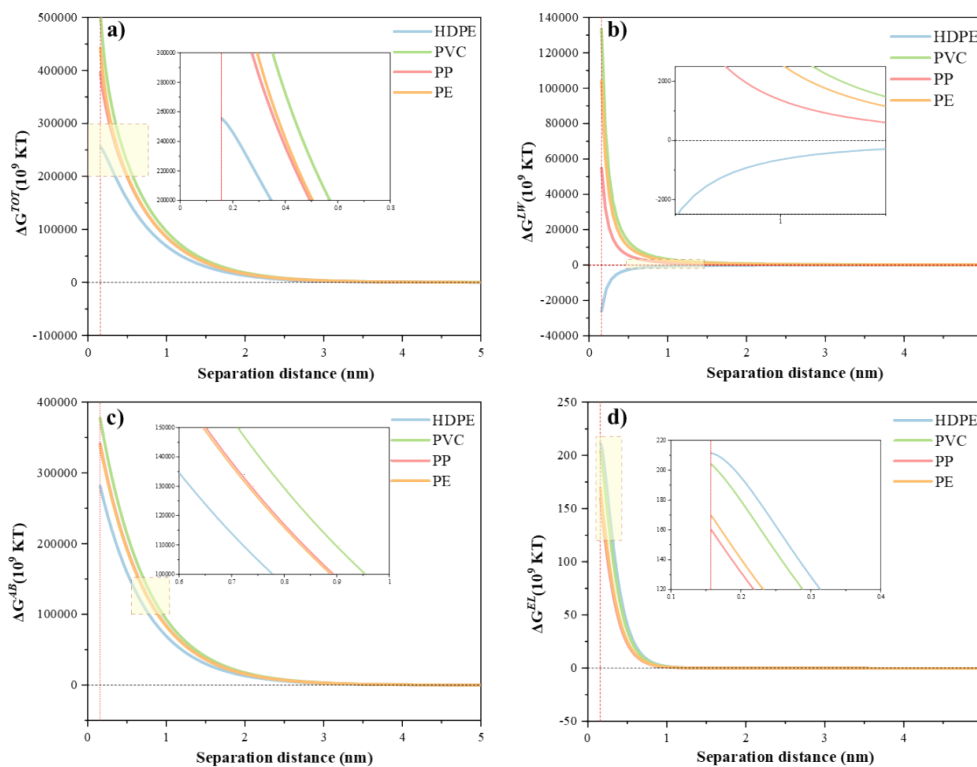
396

397 **Fig. 5** a) Contact angles of different pipe materials in three probe liquids (water, diiodomethane,  
 398 ethylene glycol). b) Surface free energy of different pipe materials, in terms of the Lifshitz-van der  
 399 Waals, acid-base, electron acceptor, and electron donor parameters. The unit for all parameters is  
 400 mJ/m<sup>2</sup>.

### 401 3.3 The interaction energy between the pipe materials and bio-clogging

402 Fig. 6 illustrates the dependence of the interaction energy between bacteria and  
 403 different pipe surfaces on the separation distance. The total interaction energy for the  
 404 four pipe materials decreased with the increase in the separation distance. In general,  
 405 the total interaction energy at minimum separation distance ( $d_0=0.158$  nm) ( $G_{d_0}^{TOT}$ ) is a  
 406 critical index of the adhesive ability of bacteria (Chen et al., 2012; Wu et al., 2020).  
 407 The  $G_{d_0}^{TOT}$  of HDPE, PVC, PP, and PE were  $2.5 \times 10^{14}$ ,  $5.2 \times 10^{14}$ ,  $4.0 \times 10^{14}$ , and  $4.5 \times$   
 408  $10^{14}$  KT, respectively. These results suggested that the bacteria preferentially adhered

409 to the HDPE owing to the lower energy barrier, consistent with the experimental  
 410 observation (Fig. 2). The high roughness decreased the interfacial energy and promoted  
 411 bio-clogging attachment (Zhao et al., 2015). Therefore, the bacteria could overcome the  
 412 lowest energy barrier ( $2.5 \times 10^{14}$  KT) in the HDPE to exhibit irreversible adhesion,  
 413 although a larger amount of bacteria adhered reversibly as they preferred to overcome  
 414 the lower energy barrier with the minimum expended energy (about 62.0 KT). For the  
 415 PVC, PP, and PE, a primary minimum expended energy was observed, suggesting that  
 416 more bacteria could adhere irreversibly.



417  
 418 **Fig. 6** Interaction energies between bacteria and pipe materials, obtained from the XDLVO analysis  
 419 of a) total interaction energy, b) van der Waals energy, c) acid-base interaction energy, and d)  
 420 electrical double-layer energy.

421 To clarify the influence of different forces on the total interaction energy, the  
 422 Lifshitz–van der Waals ( $\Delta G^{LW}$ ), acid-base ( $\Delta G^{AB}$ ), and electrostatic ( $\Delta G^{EL}$ ) interactions

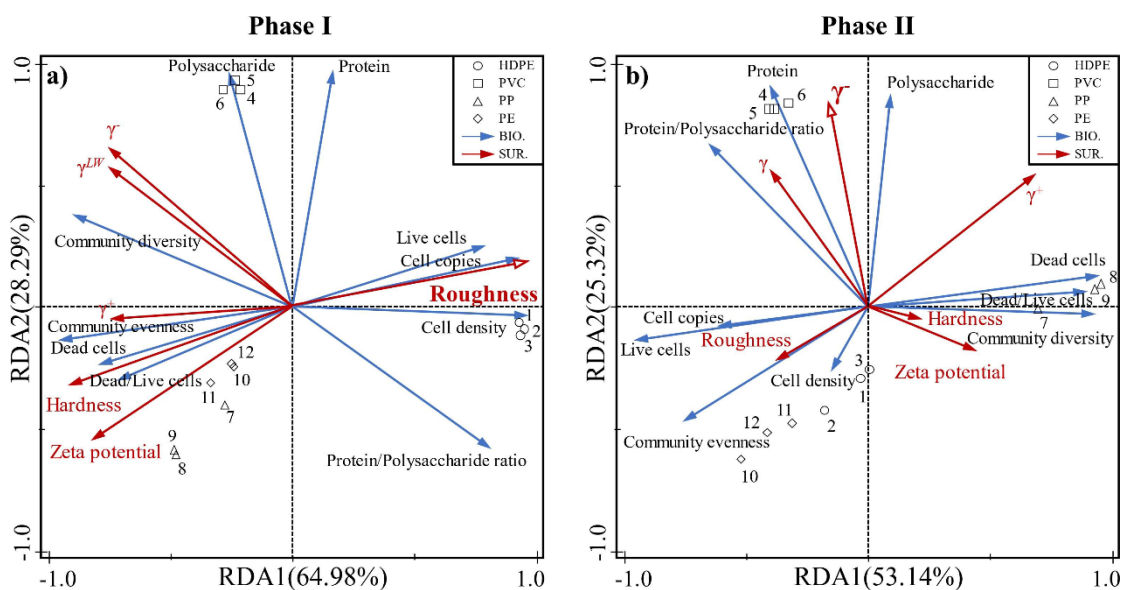
423 for the different materials were evaluated, as shown in Figs. 6b–d, respectively.  $\Delta G^{LW}$   
424 was determined by the Hamaker constant. The Hamaker constants of HDPE, PVC, PP,  
425 and PE were  $-1.08 \times 10^{-7}$ ,  $5.52 \times 10^{-7}$ ,  $2.28 \times 10^{-7}$ , and  $4.33 \times 10^{-7}$  J, respectively (Table S7).  
426 According to Eq. (9), the  $\Delta G^{LW}$  of the HDPE was negative, whereas the  $\Delta G^{LW}$  values  
427 of PVC, PP, and PE were positive. These results illustrated that strong Lifshitz–van der  
428 Waals attractive forces existed between the bacteria and HDPE, whereas repulsive  
429 effects were observed between the bacteria and other pipe materials (PVC, PP, and PE).  
430 Moreover, the  $\Delta G^{AB}$  of the different pipe materials were similar.  $\Delta G^{AB}$  exhibited the  
431 maximum energy barriers in different pipe materials, compared to  $\Delta G^{LW}$  and  $\Delta G^{EL}$ .  
432 These results suggested that repulsive Lewis acid-base interactions occurred between  
433 the bacteria and different pipe materials. In addition, the  $\Delta G^{EL}$  of different pipe  
434 materials exhibited similar trends, owing to the comparable Zeta potentials of different  
435 pipe materials (Fig. S3b). Thus, the electrostatic interaction did not considerably  
436 influence the bacterial adhesion. These results were consistent with a previous study  
437 that highlighted the absence of any significant differences in  $\Delta G^{EL}$  for different pipe  
438 materials (Cai et al., 2019). Overall, the consistency of the experimental observations  
439 with the thermodynamic prediction based on the XDLVO method demonstrated the  
440 feasibility of this approach.

### 441 **3.4 Comprehensive analysis of the relation between bio-clogging and** 442 **physicochemical properties**

443 The relationships between the bio-clogging factors and pipe material  
444 physicochemical properties in phase I and phase II were revealed by RDA (Fig. 7). In



445 phase I, RDA1 and RDA2 accounted for 65.0% and 28.3% of the bio-clogging  
446 differences in the groups, respectively. The first two axes accounted for 93.3% of the  
447 bio-clogging changes, suggesting that the surface properties indeed considerably  
448 influenced the bio-clogging characteristics. The roughness (57.6%) could explain the  
449 differences in the bio-clogging factors (Table S8). Moreover, a small angle was  
450 observed between the roughness and cell copies, suggesting a higher correlation in  
451 phase I. As illustrated in Fig. S4a, the bacterial 16 S rRNA gene of the HDPE was  
452 dominant ( $5.03 \pm 0.94 \times 10^5$  copies/cm<sup>2</sup>) among different pipe materials, consistent with  
453 the highest roughness of the HDPE (Fig. 2). The two axes also indicated a lower  
454 variability in phase II (78.4%) than that of phase I (93.3%). The predominant factors  
455 were the electron donator parameter ( $\gamma^-$ ) and electron acceptor parameter ( $\gamma^+$ ) (Table  
456 S9). A strong correlation between  $\gamma^-$  and protein was observed, supported by the fact  
457 the PVC had the highest  $\gamma^-$  (2.2 mJ/m<sup>2</sup>) and protein content ( $2623.1 \pm 33.2$   $\mu\text{g}/\text{cm}^2$ ).  
458 These results suggested that the predominant surface properties varied with phases. In  
459 the initial period, bio-clogging occurred by the adhesion of bacteria with an increase in  
460 the roughness. In the later period, the bio-clogging generation became highly complex  
461 with the secretion of proteins and polysaccharides owing to the increase in  $\gamma^-$ .



462

463 **Fig. 7** Redundancy analysis (RDA) of the relationships between the bio-clogging characteristics and

464 physicochemical properties of pipe materials in two different phases.

465 Moreover, linear correlation tests were performed to investigate the relationship

466 between the bio-clogging characteristics and pipe material physicochemical properties

467 (Fig. 8). The total surface free energy ( $\gamma$ ) was significantly correlated with the Lifshitz-

468 van der Waals component ( $\gamma^{LW}$ ) ( $R^2=1.0$ ,  $P\leq 0.001$ ), consistent with the fact that  $\gamma^{LW}$

469 was the main contributor to the  $\gamma$  value of different pipe materials (Fig. 5b).

470 Interestingly, the Zeta potential was positively correlated with the hardness ( $R^2=0.94$ ,

471  $P\leq 0.001$ ). However, limited information is available regarding the relationship

472 between the zeta potential and hardness. In phase I, both the cell density ( $R^2=0.93$ ) and

473 cell copies ( $R^2=0.94$ ) were strongly correlated with the roughness ( $P\leq 0.001$ ). These

474 results were consistent with the RDA results, indicating that roughness was the

475 predominant factor for bacterial adhesion and promoted bio-clogging formation. In

476 phase II,  $\gamma$  was positively correlated with the protein ( $R^2=0.77$ ) and

477 protein/polysaccharide ratio ( $R^2=0.73$ ), respectively ( $P\leq 0.01$ ). Thus,  $\gamma$  could stimulate



494 (2623.1±33.2 μg/cm<sup>2</sup>) were observed for the PVC. Moreover, the interaction energy  
495 indicated that the bacteria could irreversibly and reversibly adhere to the HDPE,  
496 whereas irreversible adhesion occurred on PVC, PP, and PE. This study provides a  
497 novel thermodynamic framework for the bio-clogging development in leachate for  
498 different pipe materials and can enhance the fundamental understanding of bio-  
499 clogging, thereby promoting the development of novel bio-clogging control strategies.

#### 500 **Declaration of competing interest**

501 The authors declare that they have no known competing financial interests that  
502 could have appeared to influence the work reported in this paper.

#### 503 **Acknowledgments**

504 This research was financially supported by the National Natural Science  
505 Foundation of China (22176005) and Guangdong Basic and Applied Basic Research  
506 Foundation (2021A1515110724).

507 **References:**

- 508 Alimi, O.S., Farner Budarz, J., Hernandez, L.M., Tufenkji, N., 2018. Microplastics and  
509 nanoplastics in aquatic environments: aggregation, deposition, and enhanced  
510 contaminant transport. *Environ. Sci. Technol.* 52 (4), 1704-1724.
- 511 Anand, N., Palani, S.G., 2022. A comprehensive investigation of toxicity and pollution  
512 potential of municipal solid waste landfill leachate. *Sci. Total Environ.* 838,  
513 155891.
- 514 Bradford, S.A., Sasidharan, S., Kim, H., Hwang, G., 2018. Comparison of types and  
515 amounts of nanoscale heterogeneity on bacteria retention. *Front. Environ. Sci.*  
516 6: 56.
- 517 Cai, L., Wu, D., Xia, J., Shi, H., Kim, H., 2019. Influence of physicochemical surface  
518 properties on the adhesion of bacteria onto four types of plastics. *Sci. Total*  
519 *Environ.* 671, 1101-1107.
- 520 Carrel, M., Morales, V.L., Beltran, M.A., Derlon, N., Kaufmann, R., Morgenroth, E.,  
521 Holzner, M., 2018. Biofilms in 3D porous media: delineating the influence of  
522 the pore network geometry, flow and mass transfer on biofilm development.  
523 *Water Res.* 134, 280-291.
- 524 Chen, L., Tian, Y., Cao, C.Q., Zhang, J., Li, Z.N., 2012. Interaction energy evaluation  
525 of soluble microbial products (SMP) on different membrane surfaces: role of  
526 the reconstructed membrane topology. *Water Res.* 46 (8), 2693-2704.
- 527 Dubois, M., Gilles, K.A., Hamilton, J.K., Rebers, P.A., Smith, F., 1956. Colorimetric  
528 method for determination of sugars and related substances. *Anal. Chem.* 28,

529 350–356.

530 Feng, S.J., Chen, Z.W., Zheng, Q.T., 2020. Effect of LCRS clogging on leachate  
531 recirculation and landfill slope stability. *Environ Sci Pollut Res.* 27, 6649–6658.

532 Flemming, H.C., Wingender, J., 2010. The biofilm matrix. *Nat. Rev. Microbiol.* 8 (9),  
533 623-633.

534 Ganesan, S., Ruendee, T., Kimura, S.Y., Chawengkijwanich, C., Janjaroen, D., 2022.  
535 Effect of biofilm formation on different types of plastic shopping bags:  
536 Structural and physicochemical properties. *Environ. Res.* 206, 112542.

537 Habimana, O., Semião, A.J.C., Casey, E. 2014. The role of cell-surface interactions in  
538 bacterial initial adhesion and consequent biofilm formation on  
539 nanofiltration/reverse osmosis membranes. *J. Membrane Sci.* 454, 82-96.

540 Kamatkar, N.G., Shrout, J.D., 2011. Surface hardness impairment of quorum sensing  
541 and swarming for *Pseudomonas aeruginosa*. *PLoS One.* 6 (6), e20888.

542 Ko, J.H., Wang, Q., Yuan, T., Wu, H., Xu, Q., 2019. Geotextile clogging at different  
543 stages of municipal solid waste landfills co-disposed with bottom ash. *Sci. Total*  
544 *Environ.* 687, 161-167.

545 Li, M., Zhao, R., Yang, T., Ma, S., 2021. Fabrication of anti-scaling HDPE/fluorinated  
546 acrylate polymer/nano-silica composite for landfill leachate piping system.  
547 *Chemosphere.* 284, 131302.

548 Liu, X.M., Sheng, G.P., Yu, H.Q., 2007. DLVO approach to the flocculability of a  
549 photosynthetic H<sub>2</sub>-producing bacterium, *Rhodospseudomonas acidophila*.  
550 *Environ. Sci. Technol.* 41 (492), 4620-4625.

- 551 Liu, Y., Liu, J., 2021. Mechanism and dynamic evolution of leachate collection system  
552 clogging in MSW landfills in China. *Waste Manage.* 120, 314-321.
- 553 Luo, H., Zeng, Y., Cheng, Y., He, D., Pan, X., 2020. Recent advances in municipal  
554 landfill leachate: a review focusing on its characteristics, treatment, and toxicity  
555 assessment. *Sci. Total Environ.* 703, 135468.
- 556 Ma, S., Zhou, C., Pan, J., Yang, G., Sun, C., Liu, Y., Chen, X., Zhao, Z., 2022. Leachate  
557 from municipal solid waste landfills in a global perspective: characteristics,  
558 influential factors and environmental risks. *J. Clean Prod.* 333, 130234.
- 559 Meng, F., Zhang, S., Oh, Y., Zhou, Z., Shin, H.S., Chae, S.R., 2017. Fouling in  
560 membrane bioreactors: an updated review. *Water Res.* 114, 151-180.
- 561 Merghni, A., Kammoun, D., Hentati, H., Janel, S., Popoff, M., Lafont, F., Aouni, M.,  
562 Mastouri, M., 2016. Quantification of *Staphylococcus aureus* adhesion forces  
563 on various dental restorative materials using atomic force microscopy. *Appl.*  
564 *Surf. Sci.* 379, 323-330.
- 565 Mohiuddin, M.T.K., Linnea, K.I., Gabriel, P.L., Andrew, J.S., 2011. Experimental and  
566 theoretical examination of surface energy and adhesion of nitrifying and  
567 heterotrophic bacteria using self-assembled monolayers. *Environ. Sci. Technol.*  
568 45, 1055-1060.
- 569 Niu, L., Li, Y., Li, Y., Hu, Q., Wang, C.D., Hu, J., Zhang, W., Wang, L., Zhang, C.,  
570 Zhang, H., 2021. New insights into the vertical distribution and microbial  
571 degradation of microplastics in urban river sediments. *Water Res.* 188, 116449.
- 572 Osnes, T., Sandstad, O., Osnes, V.S.M., Kierulf, P., 1993. Total protein in common

573 duct bile measured by acetonitrile precipitation and a micro bicinchoninic acid  
574 (BCA) method. *Scand. J. Clin. Lab. Invest.* 53, 757–763.

575 Rowe, R.K., Yu, Y., 2012. Clogging of finger drain systems in MSW landfills. *Waste*  
576 *Manage.* 32 (12), 2342-2352.

577 Shaha, B.N., Meeroff, D.E., Kohn, K., Townsend, T.G., Schert, J.D., Mayer, N., Schultz,  
578 R., Telson, J., 2019. Effect of electronic water treatment system on calcium  
579 carbonate scale formation in landfill leachate collection piping. *J. Environ. Eng.*  
580 145 (9), 04019052.

581 Somathilake, M., Hettiaratchi, J., 2012. Struvite formation in leachate recirculation  
582 pipes of bioreactor landfills. *J. Solid Waste Technol. Manag.* 38 (4), 291-299.

583 Sousa, C., Teixeira, P., Oliveira, R., 2009. Influence of surface properties on the  
584 adhesion of *Staphylococcus epidermidis* to acrylic and silicone. *Int. J. Biomater.*  
585 2009, 718017.

586 Syranidou, E., Karkanorachaki, K., Amorotti, F., Franchini, M., Repouskou, E., Kaliva,  
587 M., Vamvakaki, M., Kolvenbach, B., Fava, F., Corvini, P.F., Kalogerakis, N.,  
588 2017. Biodegradation of weathered polystyrene films in seawater microcosms.  
589 *Sci. Rep.* 7 (1), 17991.

590 Tang, Q., Gu, F., Zhang, Y., Zhang, Y., Mo, J., 2018. Impact of biological clogging on  
591 the barrier performance of landfill liners. *J. Environ. Manage.* 222, 44-53.

592 Tarek, A., Daria, S., 2015. Clogging of leachate collection systems in Florida.  
593 Gainesville, FL: Hinkley Center for Solid and Hazardous Waste Management.

594 Teng, J., Zhang, H., Lin, H., Lu, M., Xu, X., Gao, T., You, X., 2022. Molecular level



595 insights into the dynamic evolution of forward osmosis fouling via  
596 thermodynamic modeling and quantum chemistry calculation: Effect of  
597 protein/polysaccharide ratios. *J. Membr. Sci.* 655, 120588.

598 Teng, J., Zhang, M., Leung, K.T., Chen, J., Hong, H., Lin, H., Liao, B.Q., 2019. A  
599 unified thermodynamic mechanism underlying fouling behaviors of soluble  
600 microbial products (SMPs) in a membrane bioreactor. *Water Res.* 149, 477-487.

601 Townsend, T. G., 2015. Assessing options for on-site leachate management at Florida  
602 landfills. Gainesville, FL: Hinkley Center for Solid and Hazardous Waste  
603 Management.

604 Van Oss, C.J., 2010. *Interfacial forces in aqueous media*, New York. CRC Press.

605 Wang, Q., Ko, J.H., Wu, H., Liu, F., Xu, Q., 2021a. Impact of bottom ash co-disposed  
606 with municipal solid waste on geotextile clogging in landfills. *Sci. Total*  
607 *Environ.* 774, 145744.

608 Wang, Q., Ko, J.H., Xu, Q., 2021b. Comparison of bio-clogging characteristics of  
609 geotextiles in MSW and bottom ash co-disposal landfills. *Waste Manage.* 120,  
610 459-466.

611 Wang, Q., Liu, F., Xu, Q., 2022. Insight into the effect of calcium on bio-clogging  
612 behavior via quartz crystal microbalance with dissipation monitoring.  
613 *Chemosphere.* 133547.

614 Wu, H., Wang, Q., Ko, J.H., Xu, Q., 2018. Characteristics of geotextile clogging in  
615 MSW landfills co-disposed with MSWI bottom ash. *Waste Manage.* 78, 164-  
616 172.

617 Wu, M., Chen, Y., Lin, H., Zhao, L., Shen, L., Li, R., Xu, Y., Hong, H., He, Y., 2020.  
618 Membrane fouling caused by biological foams in a submerged membrane  
619 bioreactor: Mechanism insights. *Water Res.* 181, 115932.

620 Xu, J., Yu, H., Li, X., 2016. Probing the contribution of extracellular polymeric  
621 substance fractions to activated-sludge bioflocculation using particle image  
622 velocimetry in combination with extended DLVO analysis. *Chem. Eng. J.* 303,  
623 627-635.

624 Xu, S., Lu, W., Liu, Y., Ming, Z., Liu, Y., Meng, R., Wang, H., 2017. Structure and  
625 diversity of bacterial communities in two large sanitary landfills in China as  
626 revealed by high-throughput sequencing (MiSeq). *Waste Manage.* 63, 41-48.

627 Yan, X., Lin, T., Wang, X., Zhang, S., Zhou, K., 2022. Effects of pipe materials on the  
628 characteristic recognition, disinfection byproduct formation, and toxicity risk of  
629 pipe wall biofilms during chlorination in water supply pipelines. *Water Res.* 210,  
630 117980.

631 Yang, K., Shi, J., Wang, L., Chen, Y., Liang, C., Yang, L., Wang, L.-N., 2022. Bacterial  
632 anti-adhesion surface design: Surface patterning, roughness and wettability: A  
633 review. *J. Mater. Sci. Technol.* 99, 82-100.

634 Yin, Z., Yeow, R.J.E., Ma, Y., Chew, J.W., 2020. Link between interfacial interaction  
635 and membrane fouling during organic solvent ultrafiltration of colloidal foulants.  
636 *J. Membr. Sci.* 611, 118369.

637 Yongabi, D., Khorshid, M., Gennaro, A., Jookan, S., Duwe, S., Deschaume, O., Losada-  
638 Perez, P., Dedecker, P., Bartic, C., Wubbenhorst, M., Wagner, P., 2020. QCM-

639 D study of time-resolved cell adhesion and detachment: effect of surface free  
640 energy on Eukaryotes and Prokaryotes. *ACS Appl. Mater. Interfaces* 12(16),  
641 18258-18272.

642 Zeng, B., Pan, Z., Shen, L., Zhao, D., Teng, J., Hong, H., Lin, H., 2022. Effects of  
643 polysaccharides' molecular structure on membrane fouling and the related  
644 mechanisms. *Sci. Total Environ.* 836, 155579.

645 Zhang, H.M., Xia, J., Yang, Y., Wang, Z.X., Yang, F.L., 2009. Mechanism of calcium  
646 mitigating membrane fouling in submerged membrane bioreactors. *J. Environ.*  
647 *Sci.* 21 (8), 1066-1073.

648 Zhang, X., Zhou, X., Xi, H., Sun, J., Liang, X., Wei, J., Xiao, X., Liu, Z., Li, S., Liang,  
649 Z., Chen, Y., Wu, Z., 2019. Interpretation of adhesion behaviors between  
650 bacteria and modified basalt fiber by surface thermodynamics and extended  
651 DLVO theory. *Colloid Surf. B-Biointerfaces.* 177, 454-461.

652 Zhao, L., Shen, L., He, Y., Hong, H., Lin, H., 2015. Influence of membrane surface  
653 roughness on interfacial interactions with sludge flocs in a submerged  
654 membrane bioreactor. *J. Colloid Interface Sci.* 446, 84-90.